Materials Letters: X 5 (2020) 100038

Contents lists available at ScienceDirect

Materials Letters: X

journal homepage: www.elsevier.com/locate/mlblux

Nd:YAG laser scribed zinc oxide on semi-flexible copper foils

Guilherme Gaspar [a,b,*], Joana Rodrigues [a], António J.S. Fernandes [a], Maria R. Soares [b], Teresa Monteiro [a], Rui F. Silva [b,c], Florinda M. Costa [a]

[a] Department of Physics & i3N, University of Aveiro, Campus Universitário de Santiago, 3810-193 Aveiro, Portugal
[b] CICECO – Aveiro Institute of Materials, University of Aveiro, Campus Universitário de Santiago, 3810-193 Aveiro, Portugal
[c] Department of Materials and Ceramic Engineering, University of Aveiro, Campus Universitário de Santiago, 3810-193 Aveiro, Portugal

ARTICLE INFO

Article history:
Received 30 July 2019
Received in revised form 17 November 2019
Accepted 6 January 2020
Available online 7 January 2020

Keywords:
Zinc oxide
Copper
Laser processing
Oxidation
Spectroscopy

ABSTRACT

In this work, a novel approach to synthesise zinc oxide (ZnO) directly on flexible copper substrates is proposed.

The produced samples show a foam-like morphology made of agglomerates of small ZnO particles when processed at laser energy density of 18.0 J/cm^2. On the other hand, the samples processed at higher beam energy density, i.e. 33.2 J/cm^2, resulted in a more granular morphology, with some ZnO particles dispersed over the sample's surface.

Raman spectroscopy measurements demonstrated that this method resulted in the formation of wurtzite-ZnO crystalline phase in all samples. Room temperature photoluminescence spectroscopy analysis revealed the presence of a broad visible band in the orange-red region dominating the spectra, with a small contribution from the near band edge emission in the UV spectral region. Decreasing the beam energy fluence from 33.2 to 18.0 J/cm^2 resulted in samples with higher overall visible band intensity, in line with what was observed for their crystalline quality. Moreover, the shift of the broad band maxima towards longer wavelengths could be an indication of the possibility of tuning the visible emission according to the chosen laser processing conditions.

1. Introduction

ZnO is one of the most widely studied semiconductors due to its large potential of integration in numerous highly demand applications, including optoelectronics, biomedicine and piezoelectricity [1,2]. It is well established that crystalline ZnO thin films, which are of particular importance for electronic and optoelectronics industries, can be produced by distinct physical growth techniques [3–7]. Nevertheless, most of them still present some limitation regarding the synthesis in large substrate areas. Indeed, ZnO remains as a material to be used in a wide number of technologies, and therefore, the possibility of enhancing the scalability of its production in a cost- and time-effective way is still a research topic of interest for the scientific community.

Laser irradiation has been employed to promote melting of the surface layers in semiconductor substrates, with the aim of reordering damaged layers at the nanometre-scale level [8–10] and induce intentional phase transitions without using resistive element furnaces [11,12].

In the present work, a fast and environmentally friendly processing technique, using a neodymium-doped yttrium aluminium garnet (Nd:YAG) laser operating in the 1064 nm wavelength, was employed to produce crystalline ZnO structures directly on copper (Cu) substrates from a zinc (Zn)-based precursor formulation. Attentions were mostly devoted to the structural and optical characterisation of the produced samples and the influence of the laser processing parameters on the mentioned properties.

2. Materials and methods

2.1. Synthesis

ZnO was produced on 300 μm thick commercial copper foils. This material was chosen as substrate since it may further work as an electrical contact to a relatively flexible ZnO-based device for optoelectronic or sensing applications. A paste comprising Zn powder and polyvinyl alcohol (PVA) was firstly spread on the substrate and subsequently laser treated. The details of the paste formulation are described elsewhere (designated as Zn#1 paste) [13].

* Corresponding author at: Department of Physics & i3N, University of Aveiro, Campus Universitário de Santiago, 3810-193 Aveiro, Portugal.
E-mail address: gmmg@ua.pt (G. Gaspar).

https://doi.org/10.1016/j.mlblux.2020.100038
2590-1508/

Prior to the spreading of the Zn precursor, the Cu foils were chemically etched with standard procedures to reduce roughness and remove contaminants from the surface [14]. Approximately 63 μl/cm^2 of the precursor paste was slowly spread on the foil surface via doctor blade technique. Finally, the samples were left to dry in air for 48 h. The height step between the as-dried paste layer and the as-cleaned copper foil was measured with an optical profiler and an average precursor layer thickness of about 8 μm was thus obtained.

The laser treatment was performed with a Nd:YAG pulsed laser, with peak emission at 1064 nm (Rofin Starmark SMP 100wII). The laser system allows processing of centimetre square areas. The samples were placed at the laser focus position, resulting in a spot diameter of 50 μm, and 5 × 5 mm^2 areas were scanned for each set of parameters. The frequency was set to 17.5 kHz with pulse duration of 30 μs, while the distance between scanning lines was 100 μm. Different scan speeds (from 20 to 40 mm/s, with steps of 10 mm/s) and average laser powers (from 6.2 to 11.4 W, with steps of ~1.7 W) were used to study their impact on the ZnO formation. Considering the fixed pulse frequency and laser spot area, the present precursors were processed at energy densities from 18.0 to 33.2 J/cm^2. In addition, we aimed at relatively high processing times to promote both polymer evaporation and improved crystalline quality, so the lower limits of the system in respect to distance between scanning lines and scan speed were explored (100 μm and 20–40 mm/s, respectively). The slow scan speeds used to synthesise the samples presented below, 20 and 40 mm/s, resulted in a reduced distance between laser pulses, 1.1 and 2.3 μm, respectively. Given the laser spot diameter, the samples were synthesised with high percentage of beam overlap along each line scan.

Table 1 shows the list of samples that were selected among the produced ones for the characterisation studies, together with the corresponding laser operating conditions (i.e. average laser power, and corresponding energy density, and scan speed).

2.2. Materials characterisation

The surface morphology of the samples was inspected with a TESCAN Vega3 scanning electron microscope (SEM) using a working distance of 15.2 mm, a 25 kV accelerating voltage and 5 k× magnification. Energy-dispersive X-ray spectroscopy (EDS) was used to map the surface composition of the produce samples with a Bruker Xflash 410 M Silicon Drift Detector, 133 eV energy resolution (Mn Kα) @ 100 kcps counting rate.

Micro-Raman spectroscopy measurements were conducted in a Horiba Jobin Yvon HR800 instrument in backscattering configuration using a 600 gr/mm grating and using the 442 nm (~2.8 eV) cw He-Cd laser line (Kimmon IK Series) as excitation source. The laser light was focused on the samples by using a 50× magnification objective.

Samples #1, #2 and #3 were selected for room temperature (RT) steady-state photoluminescence (PL) spectroscopy measurements. Furthermore, excitation density-dependent measurements were also conducted on sample #3, while both samples #1 and #3 were chosen for temperature-dependent PL. In the first case, the samples were kept at 11 K and the excitation density was controlled using neutral density filters. For the temperature-dependent measurements, the samples were placed in a cold finger, and the temperature changed from 11 K to RT. All the measurements were carried out using the 325 nm (3.8 eV) line from a cw He-Cd laser with a beam spot of ~1 mm and an excitation power density less than 0.6 W/cm^2. The signal emitted from the samples was dispersed by a SPEX 1704 monochromator (1 m, 1200 g/mm) and detected with a cooled Hamamatsu R298 photomultiplier.

Table 1
List of the selected samples and corresponding laser operating conditions.

Sample	Laser power (W)	Energy density (J/cm^2)	Scan speed (mm/s)
#1	11.4	33.2	20
#2	11.4	33.2	40
#3	6.2	18.0	20
#4	6.2	18.0	40

3. Results and discussion

3.1. Morphology

Fig. 1 shows SEM micrographs of the selected samples, as well as for the reference one, i.e. copper foil covered by the Zn/PVA prior laser treatment (REF sample). It is clear from the pictures that the laser treatment step introduces significant changes in the surface morphology of the samples. The morphology of the REF sample seems to be heterogeneous at the macroscale, mostly due to the spreading technique that was used and the size of the Zn particles, resulting in the presence of some agglomerates of Zn.

After laser irradiation, the surface exhibits the presence of some agglomerates with different dimensions, as shown in Fig. 1 for samples #1 and #2. In addition, it is possible to detect small whitish round-shaped particles formed at the surface of the samples, with diameter in the order of 1 μm. These particles are more homogeneous in size and evidence a better surface dispersion for the sample processed at lower scan speed (sample #1). They are likely to correspond to small ZnO particles that are formed on the samples' surface after laser treatment. EDS mapping was performed on sample #1 to understand the distribution of the different elements. The relevant elements, Zn and oxygen (O), are seen to be well dispersed onto the surface and may indicate the formation of ZnO structures. Since the paste formulation comprised a polymeric matrix, carbon (C) was also monitored, and traces of this element are found to be well spread on the surface of the samples. The distribution of copper was also assessed, where the EDS results show a higher concentration of copper in certain areas. That can be explained by the fact that the initial Zn-based precursor layer thickness (i.e. prior laser treatment) is not homogeneous in the entire copper surface due to the paste spreading and drying process. The strong laser interaction with the initial porous surface introduced topographical differences at the microscale due to beam dimensions, distance between scan lines and beam overlap. Although the interaction of the laser with the precursor has resulted into thermal energy delivered to promote Zn phase transformation into ZnO, it was also observed that such high laser energy fluence led to the ablation of part of the precursor from the surface.

When the energy density is reduced from 33.2 to 18.0 J/cm^2, the morphology of the samples is rather different from the ones processed at higher energy density. Here, the morphology of the as-spread surface is by some means maintained while large agglomerates are mainly formed after laser treatment. These agglomerates seem to be made of smaller ones, likely to be ZnO particles, due to the rather moderate (i.e. pure thermal) interaction between the laser beam and the precursor paste. Regarding the PVA, it is expected that it fully decomposes for the laser energy densities that have been used [15], although traces of carbon are simultaneously present with ZnO.

3.2. Raman spectroscopy

Representative Raman spectra for samples #1 to #4 are shown in Fig. 2, which also includes the spectrum obtained for the REF

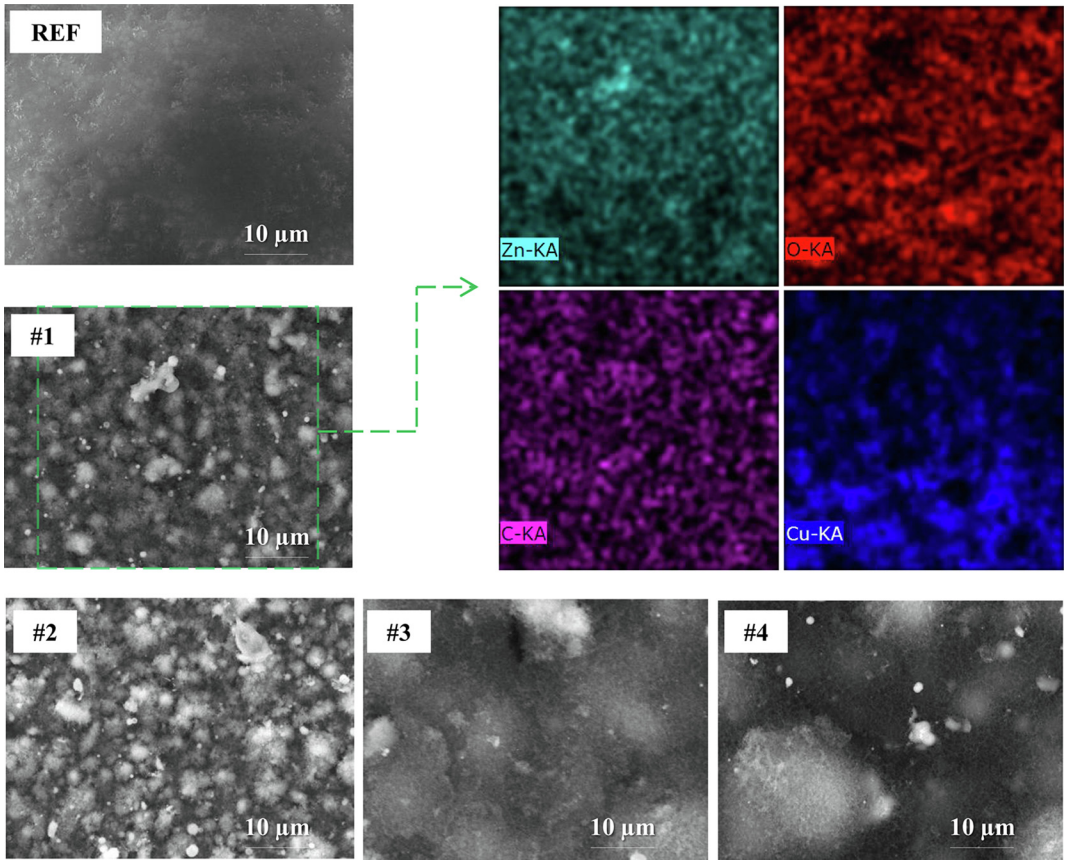

Fig. 1. SEM micrographs of the Zn/PVA paste spread on substrate (REF sample) prior the laser treatment and of all produced samples after laser treatment. The distribution of zinc, oxygen, carbon and copper elements is also shown for the corresponding micrograph of #1 (area inside the dashed line).

sample for comparison. Raman active vibrational modes of the ZnO wurtzite phase were identified in the laser treated samples, namely the A_1, E_1 and E_2 modes, as well as their overtones and combined modes [16].

The reference sample also exhibits some traces of ZnO phase, namely the $A_1(LO)$, $2E_1(LO)$, which should be due to the natural oxidation of the Zn precursor, further promoted by the local heating resultant from the focused laser incidence. The other peaks, in the

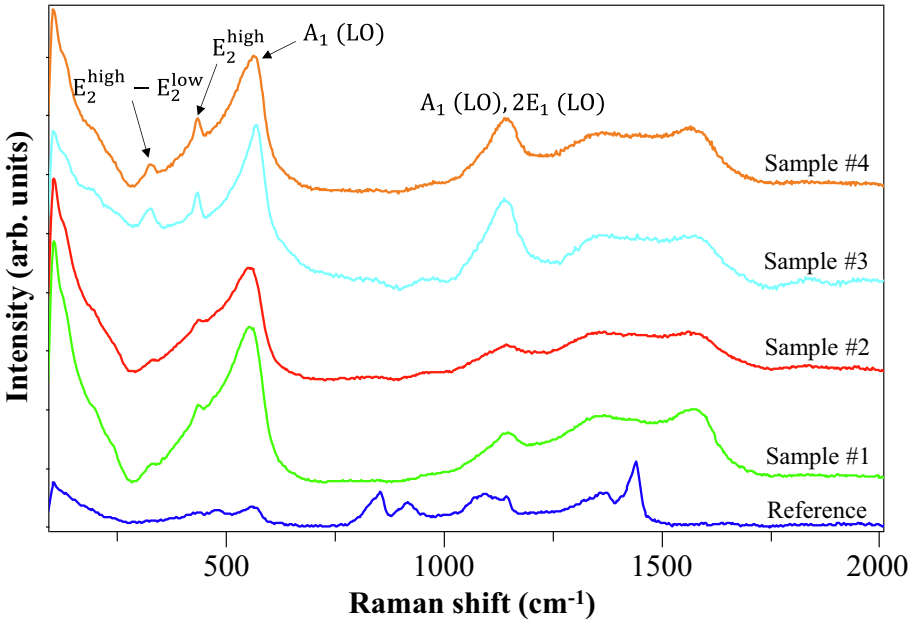

Fig. 2. Representative Raman spectra for the laser treated samples as well as for the reference sample, all obtained under 442 nm laser line excitation.

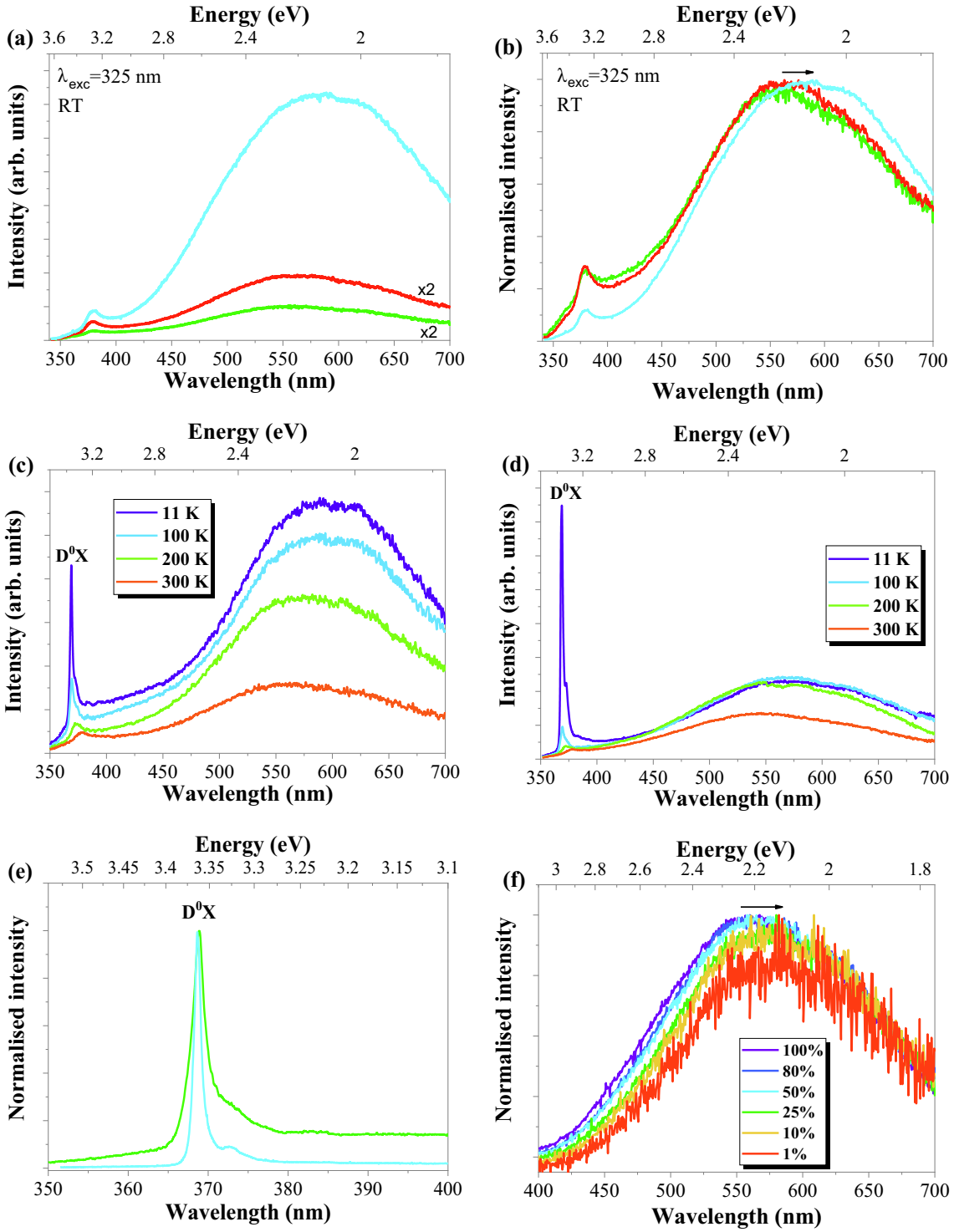

Fig. 3. Representative RT PL spectra of the as-annealed samples excited with a 325 nm laser line, showing the (a) absolute and (b) normalised PL intensity. The colour coding comprises green, red and light blue and correspond to samples #1, #2 and #3, respectively. Temperature-dependent PL spectra for (c) sample #1 and (d) sample #3. (e) NBE range (high resolution) spectra measured at 11 K for both #1 and #3. (f) Density-dependent normalized PL spectra acquired at 11 K for sample #3. (For interpretation of the references to colour in this figure legend, the reader is referred to the web version of this article.)

range of 750–1500 cm^{-1}, can be associated to PVA Raman modes [17]. After laser treatment, the PVA-related peaks completely vanish, and broad and overlapped modes, peaking at ~1349 cm^{-1} and ~1564 cm^{-1}, arise, together with the ZnO wurtzite modes. The former ones (D and G bands, respectively) indicate the presence of amorphous carbon in the produced ZnO structures [18].

The broad peaks observed in the ZnO case may be accounted by some amorphous phases or higher density of defects. For instance, the existence of non-stoichiometric ZnO_x phases or the mentioned residual metallic Zn with some spontaneously formed native oxide may contribute to this broadening, pointing out towards a low degree of crystallinity in the formed ZnO.

Moreover, no major differences were observed between the results for the two different laser scan speeds. Nevertheless, the E_2^{high} and $A_1(LO)$ longitudinal optical modes can be clearly identified, with a predominance of the later. According to SEM observations, only small ZnO particles are formed (being spread over large areas), which, together with the highly defective films, may also contribute to the relatively weak ZnO-related peak intensities that are found. This can be explained by the fact that, at high fluences, the laser contributes to the ablation and digging of the initial porous structure and only part of the energy is used for the Zn phase transformation into ZnO.

On the other hand, the same does not happen to the samples processed at 18.0 J/cm^2 (sample #3 and #4), where the E_2^{high} peak and the corresponding combination with E_2^{low} are clearly visible. An increase in the intensity of these modes for samples processed at 18.0 J/cm^2 may thus be attributed to the presence of ZnO particles of higher crystallinity. Indeed, the E_1 and E_2 related modes intensity and width, as the ones measured for these samples, are comparable to ZnO synthesised with other physical methods, like RF sputtering [3], or solution processed methods [19–21].

3.3. Photoluminescence spectroscopy

The selected samples for PL were analysed by exciting them with a laser beam of 325 nm (~3.8 eV), which is above the energy bandgap of ZnO (3.3 eV at RT) [22]. Fig. 3(a) and (b) shows representative RT PL spectra for the selected samples. It is worth to note that the optical alignment was kept for all samples to allow direct comparison between the absolute intensity of their PL signal. In all cases, the spectra were dominated by a broad band covering most of the visible spectral range (from ~400 to 700 nm). Additionally, a small contribution from the near band edge (NBE) emission in the UV spectral region could also be detected. Broad luminescent bands in the visible range, such as the ones identified in the present spectra, are typically found in ZnO structures due to the presence of several intrinsic and extrinsic defects [23–25]. Moreover, surface-related defects have also been accounted for giving rise to broad visible bands, especially in the green and yellow spectral regions [26–28,7]. Nevertheless, the nature of these defects remains unclear, especially because different defect centres are known to originate PL bands peaked at the same spectral regions. Thus, these bands are comprised by an overlap of several recombination channels, giving rise to radiative recombination in similar spectral region [13,22,27].

Probing the samples in different spots does not show major differences in the peak position or spectral shape of the bands, suggesting a rather homogeneous emission through the samples. Inspection of Fig. 3(a) seems to point towards a slight increase of the PL intensity with increasing scan speed. Furthermore, when the laser beam intensity is reduced to 18.0 J/cm^2 during the synthesis step, the overall visible band intensity increases substantially. Moreover, a shift of approximately 40 nm towards longer wavelengths is detected for sample #3 (Fig. 3(b)). While the broad band is centred at approximately 550 nm for both samples #1 and #2, the broad band peaks at approximately 590 nm in sample #3. Therefore, laser treatment at 18.0 J/cm^2, seems to lead to ZnO that emits preferentially at longer wavelengths, while processing at 33.2 J/cm^2 seems to promote the optical centres whose emission is mainly peaked at the green-yellow spectral region. The predominant orange-red emission observed for samples #3 may be related with the introduction of oxygen-related defects, since this band is frequently attributed to the interstitial oxygen [29,30], and may be promoted due to the samples' synthesis in air. Nowadays, it is well accepted that one of the charge states of zinc vacancies and their aggregates give rise to electronic levels between 1.6 and 2.1 eV below the conduction band [31,32]. In our case, the formation of such defects may arise from the fast laser treatment and the limited air exposure of the Zn precursor that remains beneath the already formed ZnO.

Fig. 3(c) and (d) shows temperature-dependent PL spectra of samples #1 and #3, respectively. It is interesting to note that the relative intensity of the NBE emission regarding the visible one is different in the two samples, with the former dominating the spectra for sample #3. The ratio between the NBE recombination and the deep level emission constitutes an indication of the optical quality of the samples. At 11 K, an intensity ratio of ~0.8 was found for sample #1, while sample #3 exhibit a ratio of ~3, indicating a higher optical quality of the ZnO produced in the conditions of sample #3. At low temperatures the UV emission peaks at 369 nm (~3.4 eV), which is due to the overlap of the free exciton (FX) and several emitting donor-bound excitons (D^0X, I_i lines) [33–35]. Higher resolution spectra are depicted in Fig. 3(e). The asymmetry observed for higher wavelength region is likely due to the contribution of other defect centres, namely the surface related defects [36]. The higher broadening evidenced by sample #1 in this region seems to indicate a higher density of such defects, in line with the NBE/visible emission ratio observed. Nevertheless, the observation of this well-resolved NBE recombination confirms the formation of ZnO structures with good optical quality. The higher relative intensity of the NBE emission in sample #3 may also be accounted by the presence of residual carbon. Therefore, its presence is likely to contribute to the higher relative intensity of the visible PL band *vs* NBE intensity [37]. In the present samples, a small peak can be identified at ~372 nm (~3.3 eV), which can be related with Y-line transition, which is attributed to the recombination of excitons bound to unknown donor defects [38].

As the temperature increases, the overall PL intensity decreases and the NBE emission shifts towards longer wavelengths. Increasing the temperature promotes the dissociation of the bound excitons, and, at RT, the emission is dominated by an overlap of the transitions associated with the FX and the surface-related defects. In the case of the broad emission, its peak position slightly shifts towards shorter wavelengths as the temperature increases. Such behaviour is likely related with the presence of multiples recombination channels, whose relative intensity changes as the temperature increases. This assumption was also corroborated by the slight shift of the band position as a function of the excitation density, as displayed in Fig. 3(f).

4. Conclusions

We have successfully synthesised ZnO directly on copper substrates using a fast and facile route that comprises the use of a Nd:YAG infrared laser able to scan large surface areas. The morphology of the samples processed at laser energy density of 33.2 J/cm^2 seemed to be made of large agglomerates of unprocessed Zn, with some ZnO particles dispersed over the surface, while the samples processed under lowest energy density, i.e. 18.0 J/cm^2, show agglomerates/webs made of small ZnO particles.

Raman spectroscopy revealed the presence of the typical active vibrational modes of the ZnO wurtzite crystalline structure, with the $A_1(LO)$ peak dominating the spectra. The Raman modes seem to become better defined and less broad with the decrease of the laser energy density.

PL spectroscopy revealed that when the samples are processed at 18.0 J/cm^2, they present the highest intensity. Low temperature measurements show a well-defined NBE emission for both analysed samples, with the higher NBE/visible band ratio in the case of the samples processed with lower energy density. Such results attest the higher optical quality of the ZnO materials produced at

18.0 J/cm^2, allied to the high percentage of laser beam overlap employed.

Declaration of Competing Interest

The authors declare that they have no known competing financial interests or personal relationships that could have appeared to influence the work reported in this paper.

Acknowledgements

The authors acknowledge financial support from FEDER funds through the COMPETE 2020 Programme and National Funds through FCT – Portuguese Foundation for Science and Technology under the projects UID/CTM/50025/2019 and POCI-01-0145-FEDER-028755.

References

[1] A. Kolodziejczak-Radzimska et al., Materials 7 (2014) 2833–2881.
[2] M. Godlewski et al., Low Temp. Phys. 37 (2011) 235.
[3] A. Ismail et al., J. King Saud Univ. Sci. 25 (2013) 209–215.
[4] P. Romero-Gomez et al., J. Phys. Chem. C 114 (2010) 20932–20940.
[5] H. Beh et al., Phys. Status Solidi A 215 (2018) 1700880.
[6] O.A. Fouad et al., Appl. Catal. B: Environ. 62 (2006) 144–149.
[7] J. Rodrigues et al., CrystEngComm 21 (2019) 1071–1090.
[8] V.P. Godbole et al., Bull. Mater. Sci. 11 (1988) 97–108.
[9] A.G. Cullis, Rep. Prog. Phys. 48 (1985) 1155–1233.
[10] F. Cristiano et al., Mat. Sci. Semicon. Proc. 42 (2016) 188–195.
[11] Y. Siegal et al., Annu. Rev. Mater. Sci. 25 (1995) 223–247.
[12] M.C. Joliet et al., Appl. Phys. Lett. 46 (1985) 266.
[13] J. Rodrigues et al., Nanoscale Adv. (2019).
[14] P. Walker et al., CRC Handbook of Metal Etchants, first ed., CRC Press, 1990.
[15] Z. Peng et al., Polym. Degrad. Stab. 92 (2007) 1061–1071.
[16] R. Cuscó et al., Phys. Rev. B 75 (2007) 165202.
[17] G.-M. Liao et al., J. Membrane Sci. 485 (2015) 17–29.
[18] A.C. Ferrari et al., Phys. Rev. B 61 (2000) 14095–14107.
[19] M. Wang et al., Sci. Rep. 5 (2015) 12925.
[20] W.-H. Chen et al., RSC Adv. 6 (2016) 91216–91224.
[21] S.A. Bidier et al., J. Mater. Sci.: Mater. Electron. 28 (2017) 11178–11185.
[22] U. Özgür et al., J. Appl. Phys. 98 (2005) 041301.
[23] T. Moe Børseth et al., Appl. Phys. Lett. 89 (2006) 262112.
[24] P. Erhart et al., Phys. Rev. B 73 (2006) 115207.
[25] R. Dingle, Phys. Rev. Lett. 23 (1969) 579.
[26] A.B. Djurišić et al., Appl. Phys. Lett. 88 (2006) 103107.
[27] A.B. Djurišić et al., Nanotechnology 18 (2007) 095702.
[28] D. Li et al., Appl. Phys. Lett. 85 (2004) 1601–1603.
[29] S.A. Studenikin et al., J. Appl. Phys. 84 (1998) 2287.
[30] W.M. Kwok et al., Appl. Phys. Lett. 87 (2005) 093108.
[31] L.J. Brillson et al., Phys. Status Solidi 9 (2012) 1566–1569.
[32] Y. Dong et al., Phys. Rev. B 81 (2010) 081201.
[33] M.R. Wagner et al., Microelectron. J. 40 (2009) 289–292.
[34] B.K. Meyer et al., Phys. Status Solidi (b) 241 (2004) 231–260.
[35] T. Monteiro et al., J. Appl. Phys. 98 (2005) 013502.
[36] J. Rodrigues et al., Sci. Rep. 5 (2015) 10783.
[37] J. Rodrigues et al., Mater. Sci. Eng., B 195 (2015) 38–44.
[38] F. Mohammadbeigi et al., J. Appl. Phys. 116 (2014) 053516.